Charge extraction and photocurrent in organic bulk heterojunction solar cells

Andreas Petersen,[1,*] Thomas Kirchartz,[2] and Thomas A. Wagner[1]
[1]*Robert Bosch GmbH, Robert-Bosch-Platz 1, D-70839 Gerlingen-Schillerhöhe, Germany*
[2]*Blackett Laboratory of Physics, Imperial College, South Kensington, London SW7 2AZ, United Kingdom*
(Received 23 October 2011; published 17 January 2012)

The pseudo point-symmetry of the photocurrent-voltage characteristics $J_{ph}(V)$ (defined as the difference between light and dark currents) has been utilized to determine important properties of organic bulk-heterojunction (BHJ) solar cells, e.g., contact recombination velocities, the dominant charge recombination mechanism, or the presence of a field dependent exciton dissociation process. In order to improve the theoretical understanding of the photocurrent generation in BHJ solar cells, we apply a numerical drift-diffusion model to investigate the effect of injection barriers, selective contacts, different recombination mechanisms, and series resistances on $J_{ph}(V)$. We show the consistency of the model with experimental data from literature and reduce different experimental observations to a single, fundamental mechanism in solar cells with intrinsic absorber layers: position dependent equilibrium concentrations and lifetimes of the charge carriers. Based on this result, we discuss the special points of the photocurrent-voltage characteristic such as the point of symmetry and the compensation voltage.

DOI: 10.1103/PhysRevB.85.045208 PACS number(s): 88.40.jr, 73.50.Pz, 73.50.Gr, 88.40.fc

I. INTRODUCTION

Organic solar cells reach power conversion efficiencies of about 8% and are considered a low cost alternative for sustainable energy generation.[1,2] In order to further enhance the efficiency of these devices, it is necessary to obtain a detailed understanding of the processes leading from the absorption of photons to the extraction of free charge carriers. The whole process of charge generation and extraction manifests itself in the cell's photocurrent density

$$J_{ph}(V) = J_{illum}(V) - J_{dark}(V). \quad (1)$$

It is defined as the difference between the current densities measured under illumination J_{illum} and in the dark J_{dark}. In *pn*-junction solar cells J_{ph} is determined by the diffusion of minority charge carriers toward the *pn*-junction.[3] As long as the series resistance R_s has a negligible effect and the applied voltage V is less than the *pn*-junction's built-in voltage V_{bi}, this diffusion driven photocurrent is approximately constant and equal to the short-circuit current density J_{sc}.[4] In contrast, J_{ph} of solar cells with an intrinsic active layer, like the organic bulk heterojunction (BHJ) and other pin-type solar cells, is affected by the internal electric field and thus depends on the applied voltage V.[5]

For organic BHJ solar cells, $J_{ph}(V)$ was reported to change sign at the compensation voltage V_0, i.e., $J_{ph}(V_0) = 0$.[6] Measurements of $J_{ph}(V)$ were utilized to determine important device properties like the contacts' selectivity,[7] the presence of a field dependent exciton dissociation process,[8,9] and the dominant recombination mechanism.[10,11] Several of these articles based their line of argument on the approximate point symmetry of $J_{ph}(V)$.[7–9] While the point of symmetry (POS) was simply defined as the center point of inflection of $J_{ph}(V)$,[8] its physical meaning and significance are still under discussion. It was proposed that the POS occurred at quasi-flat-band (QFB) conditions, i.e., at the applied voltage where the internal electric field vanished.[7–9] This idea stands in contrast to previous publications that stated that a vanishing internal electric field resulted in zero driving force for the photogenerated charge carriers and thus corresponded to the compensation voltage V_0.[6,12–14] Current density J_{POS} and voltage V_{POS} at the POS were found to be affected by thermal cell annealing and the choice of cathode material.[7,9] A large value of J_{POS} was proposed to be beneficial for a high power conversion efficiency and was suggested as an objective for cell optimization.[7,9]

The photocurrent density's offset J_{POS} was attributed to a constant diffusion current caused by self-selective contacts, i.e., an electron blocking anode and a hole blocking cathode.[7,8] Later, this theory was discarded because J_{POS} did not follow an inverse device thickness dependence as expected for a diffusion driven current.[9] Another theory for the origin of J_{POS} was a field activated exciton dissociation in the band bending regions close to the contacts.[9] While changes of the cathode material were found to alter J_{POS} by up to 50% of the maximum photocurrent density measured at reverse bias, the spatial extent of the cathode band bending region only accounted for about 10% of the total cell thickness.[9] Thus the explanation based on a field activated exciton dissociation requires a significant portion of the total optical generation to take place in the vicinity of the metallic back contact. Additionally, the weak effect of the device thickness on the shape of the photocurrent-voltage characteristics $J_{ph}(V)$ (Ref. 9) contradicts a significant influence of a field dependent charge generation mechanism.[15,16]

This paper presents a comprehensive study of the photocurrent-voltage characteristics $J_{ph}(V)$ of BHJ solar cells by means of drift-diffusion device simulation. We investigate the influence of injection barriers, selective contacts, different recombination mechanisms, and series resistances on the competition between extraction and nongeminate recombination of free charge carriers. We show our model's consistency with experimental data from Refs. 7–9, and we reduce different experimental observations to a single, fundamental mechanism in solar cells with intrinsic absorber layers: position dependent equilibrium concentrations and lifetimes of the charge carriers. Based on this result, we discuss the special points of $J_{ph}(V)$ such as the point of symmetry (POS) and the compensation voltage V_0.

II. THEORY

A. Numerical model

The presented simulations were performed by numerically solving the one-dimensional differential equation system of the continuity equations for electrons and holes,

$$\frac{\partial J_{\mathrm{n}}}{\partial x} = -q[G(x) - R(x)], \tag{2}$$

$$\frac{\partial J_{\mathrm{p}}}{\partial x} = q[G(x) - R(x)], \tag{3}$$

and the Poisson equation

$$\Delta\varphi = -\frac{\rho}{\epsilon_0\epsilon_{\mathrm{r}}}, \tag{4}$$

which relates the electrical potential φ to the space charge ρ, the dielectric constant ϵ_0, and the relative permittivity ϵ_{r}. Here, $G(x)$, $R(x)$, and q denote the optical generation rate, the recombination rate, and the elementary charge, respectively. Assuming bandlike transport, the current densities were expressed by drift and diffusion,

$$J_{\mathrm{n}} = q\left(n\mu_{\mathrm{n}}F + D_{\mathrm{n}}\frac{\partial n}{\partial x}\right), \tag{5}$$

$$J_{\mathrm{p}} = q\left(p\mu_{\mathrm{p}}F - D_{\mathrm{p}}\frac{\partial p}{\partial x}\right), \tag{6}$$

where the diffusion constants $D_{\mathrm{n,p}}$ were assumed to be related to the electron and hole mobilities $\mu_{\mathrm{n,p}}$ by the Einstein relation $D_{\mathrm{n,p}} = \mu_{\mathrm{n,p}}k_{\mathrm{B}}T/q$. The concentrations of electrons and holes are labeled n and p while F, T, and k_{B} denote the electric field, the temperature, and the Boltzmann constant, respectively. In this framework, bulk heterojunction (BHJ) cells were modeled as an active layer in between two electrodes. The active layer was treated as an effective medium with a band gap E_{g}, defined as the energy difference between the lowest unoccupied molecular orbital (LUMO) of the acceptor molecules and the highest occupied molecular orbital (HOMO) of the donor molecules. This approach has been widely used to model organic solar cells.[17–25]

In literature, the dominant recombination mechanism of most organic heterojunction (HJ) solar cells was assumed to be a direct recombination of free charge carriers.[18] The corresponding recombination rate

$$R_{\mathrm{direct}} = k_{\mathrm{rec}}\left(np - n_{\mathrm{i}}^2\right) \tag{7}$$

features a prefactor k_{rec} according to the Langevin theory,[26]

$$k_{\mathrm{rec}} = \frac{q(\mu_{\mathrm{n}} + \mu_{\mathrm{p}})}{\epsilon_0\epsilon_{\mathrm{r}}}. \tag{8}$$

Here, $n_{\mathrm{i}} = \sqrt{N_{\mathrm{c}}N_{\mathrm{v}}}\exp[-(qE_{\mathrm{g}})/(2k_{\mathrm{B}}T)]$ is the intrinsic charge-carrier concentration, and N_{c}, N_{v} are the effective densities of states (DOS) of LUMO and HOMO, respectively. A recombination process described by Eq. (7) results in an ideality factor $n_{\mathrm{id}} = 1$ and cannot account for the typical ideality factors of organic solar cells $n_{\mathrm{id}} > 1$.[27] One explanation for $1 \leqslant n_{\mathrm{id}} \leqslant 2$ is a trap assisted recombination process.[27] For the simulation, it was taken into account in the form of a Shockley-Read-Hall (SRH) recombination rate R_{SRH} for a single deep defect,[28,29]

$$R_{\mathrm{SRH}} = \frac{np - n_{\mathrm{i}}^2}{(n + p)\tau_{\mathrm{SRH}}}. \tag{9}$$

The minority charge-carrier lifetime τ_{SRH} was assumed to be identical for electrons and holes. The total recombination rate $R = R_{\mathrm{direct}} + R_{\mathrm{SRH}}$ was taken as the sum of direct and SRH recombination rates.

While it is well known that field dependent charge-carrier generation mechanisms can cause a pronounced voltage dependence of the photocurrent $J_{\mathrm{ph}}(V)$,[6,18,30] the effect of nongeminate recombination on $J_{\mathrm{ph}}(V)$ has not been investigated in detail. The influence of nongeminate recombination on $J_{\mathrm{ph}}(V)$ is especially important because different polymer solar cells were found to exhibit negligible geminate recombination.[31,32] Additionally, organic BHJ solar cells made of several state-of-the-art donor/acceptor combinations have been successfully modeled without a field dependent geminate recombination mechanism.[25,27,33,34] For this reason, a field dependent geminate recombination mechanism was not incorporated into the model.

At the contacts, current densities for electrons $J_{\mathrm{contact,n}}$ and holes $J_{\mathrm{contact,p}}$, representing extraction, injection, and recombination are given by

$$J_{\mathrm{contact,(n,p)}} = qS(n, p - n_0, p_0). \tag{10}$$

The contact behavior is determined by the surface recombination velocity S and the charge-carrier equilibrium concentrations n_0 and p_0. They are related to the electron and hole injection barriers ϕ_{n} and ϕ_{p} via Fermi statistics (in this work the Boltzmann approximation was used). For the cathode, located at the position $x = d$ where d denotes the device thickness, the equilibrium concentrations n_0 and p_0 read

$$n_0(d) = N_{\mathrm{c}}\exp\left(\frac{-\phi_{\mathrm{n}}}{k_{\mathrm{B}}T}\right) \tag{11}$$

and

$$p_0(d) = N_{\mathrm{v}}\exp\left(\frac{-E_{\mathrm{g}} + \phi_{\mathrm{n}}}{k_{\mathrm{B}}T}\right). \tag{12}$$

Analogous expressions exist for the anode located at $x = 0$. At each contact the charge carriers with the higher equilibrium concentration, i.e., electrons at the cathode and holes at the anode, are called majorities and have a surface recombination velocity $S = S_{\mathrm{maj}}$. Consequently the charge carriers with the lower equilibrium concentration are called minorities and have a surface recombination velocity $S = S_{\mathrm{min}}$.

In order to exclude effects caused by a spatially asymmetric charge-carrier generation rate, the optical generation rate $G(x) = G$ was assumed to be homogeneous. The simulations were performed employing the commercial device simulation package ASA.[35] Unless noted otherwise, the set of model parameters summarized in Table I was used.

B. Position dependent charge-carrier lifetimes

A key concept utilized in this paper is the correlation between the minority charge carriers' lifetime and their equilibrium concentration. The charge-carrier concentrations

TABLE I. Basic parameter set used in the simulations. The SRH lifetime $\tau_{SRH} = 1 \times 10^{-6}$ s was chosen according to a mobility lifetime product $\mu\tau$ of 1×10^{-14} m^2 V^{-1} (Ref. 36) and the spatially constant generation rate $G = 6.3 \times 10^{27}$ m^{-3} s^{-1} corresponds to an optically generated current density of $J_{opt} = qGd \approx 10$ mA cm^{-2}. The remaining parameters were taken from Ref. 9. An infinite contact recombination velocity $S = \infty$ was numerically represented as $S = 1 \times 10^7$ m s^{-1}.

Parameter	Symbol	Value
Effective band gap	E_g	1.1 eV
Effective DOS	N_c, N_v	1×10^{26} m^{-3}
Electron mobility	μ_n	1×10^{-8} m^2 V^{-1} s^{-1}
Hole mobility	μ_p	1×10^{-8} m^2 V^{-1} s^{-1}
Direct rec. constant	k_{rec}	1.06×10^{-16} m^3 s^{-1}
SRH lifetime	τ_{SRH}	1×10^{-6} s
Relative static permittivity	ϵ_r	3.4
Optical generation rate	G	6.3×10^{27} m^{-3} s^{-1}
Active layer thickness	d	100 nm
Temperature	T	300 K
Contact injection barriers:		
Electrons at the cathode	ϕ_n	0.1 eV
Holes at the anode	ϕ_p	0.1 eV
Contact recombination velocities:		
Majority charge carriers	S_{maj}	1×10^7 m s^{-1} (∞)
Minority charge carriers	S_{min}	1×10^7 m s^{-1} (∞)

for electrons $n = n_0 + \Delta n$ and holes $p = p_0 + \Delta p$ are given by the sum of the equilibrium concentrations n_0, p_0 and the concentrations of the excess charge carriers Δn, Δp. At the contacts, n_0 and p_0 scale exponentially with the injection barriers [see Eqs. (11) and (12)]. For sufficiently small injection barriers $\phi_{n,p}$, the equilibrium concentrations of the majority charge carriers n_0, p_0 next to the contacts exceed the local excess charge-carrier concentrations Δn, Δp. Close to the cathode, for example, $n_0 \gg p_0$ and $n_0 \gg \Delta n$. This leads to $n \approx n_0$ and $p = p_0 + \Delta p$. Combined with the identity $n_i^2 = n_0 p_0$, Eq. (7) can be simplified, yielding an expression for the direct bulk recombination rate of minority charge carriers R_{min} in the vicinity of the cathode,

$$R_{min} = \frac{\Delta p}{\tau_p}. \tag{13}$$

Here, the lifetime of holes (minorities) is given by

$$\tau_p = \frac{p_0}{k_{rec} n_i^2}. \tag{14}$$

An analogous expression exists for the lifetime of electrons τ_n in the vicinity of the anode.

Equation (14) implies that a direct recombination mechanism results in minority charge-carrier lifetimes τ_n, τ_p, which are proportional to the respective charge carrier's equilibrium concentration n_0, p_0. Consequently, in an intrinsic absorber material sandwiched between electrodes with different injection barriers, the charge carriers' equilibrium concentrations vary over the device thickness, and the recombination losses depend on the distribution of the minority charge carriers. Note that Eq. (14) represents the limiting case of Eq. (7) for large differences between the electron and hole equilibrium concentrations, i.e., for $n_0 \gg p_0$ or for $p_0 \gg n_0$. For this reason it is valid for small injection barriers and close to the contacts. At voltages around V_0, where no or small driving forces act on the photogenerated charge carriers, a significant portion of the photogenerated charge carriers recombine in the bulk of the cell and thus not close to the contacts. In this case the recombination obeys Eq. (7) and/or Eq. (9). However, if the charge carriers are effectively transported toward the contacts, i.e., if $|V| \gg V_0$, Eq. (14) is a good approximation for the charge-carrier lifetime due to direct recombination.

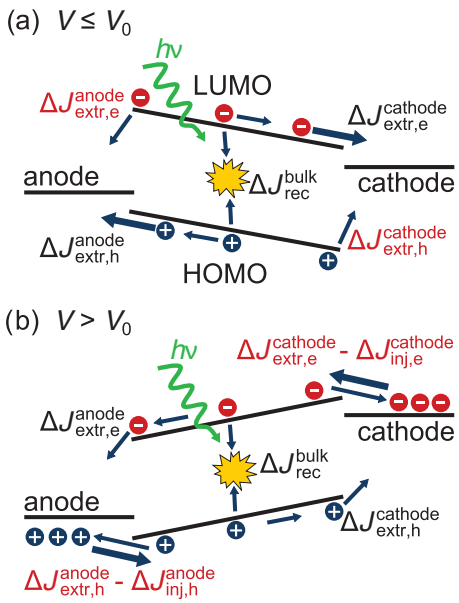

FIG. 1. (Color online) Schematic of the band structure displaying different contributions of the photocurrent density J_{ph} and the photorecombination current density ΔJ_{rec} for (a) $V \leqslant V_0$ and (b) $V > V_0$, where V_0 is the compensation voltage.

The compensation voltage V_0 is defined as the voltage where the photocurrent density vanishes, i.e., $J_{ph}(V_0) = 0$. If the cell is operated at $V < V_0$, the photogenerated charge carriers are driven toward the contacts where they are majorities, i.e., electrons toward the cathode and holes toward the anode [see Fig. 1(a)]. Because the recombination process is limited by the concentration of the minority charge carriers, the lifetime of the majority charge carriers can be considered as infinite. In contrast, for voltages $V > V_0$ the photogenerated charge carriers are driven toward the contacts where they are minorities [see Fig. 1(b)]. Due to the finite lifetime of the minority charge carriers, the extraction of minority charge carriers, i.e., $V > V_0$ and $J_{ph} > 0$, is associated with much higher recombination losses than the extraction of majorities, i.e., $V < V_0$ and $J_{ph} < 0$. These recombination losses are characterized by the photorecombination current density

$$\Delta J_{rec}(V) = J_{rec,illum}(V) - J_{rec,dark}(V). \tag{15}$$

It is defined as the difference between the recombination current densities under illumination and in the dark and can be divided into bulk and contact photorecombination current densities

$$\Delta J_{rec}(V) = \Delta J_{rec}^{bulk}(V) + \Delta J_{rec}^{contact}(V). \tag{16}$$

For the anode located at $x = 0$ and the cathode located at $x = d$, the bulk photorecombination current density

$$\Delta J_{\mathrm{rec}}^{\mathrm{bulk}}(V) = q \int_0^d R_{\mathrm{illum}}(V,x) - R_{\mathrm{dark}}(V,x)dx \quad (17)$$

can be written as the difference between the spatially integrated recombination rates under illumination R_{illum} and in the dark R_{dark}. Similarly, the contact photorecombination current density $\Delta J_{\mathrm{rec}}^{\mathrm{contact}}(V)$ is defined as the difference between the contact recombination current densities [see Eq. (10)] under illumination and in the dark. Because Eq. (10) describes both charge extraction and recombination at the contacts, only those charge extraction current densities which have a sign opposite to that of the photocurrent density $J_{\mathrm{ph}}(V)$ contribute to the contact recombination current density. Thus for $V < V_0$ the contact photorecombination current density reads [see Fig. 1(a)]

$$\Delta J_{\mathrm{rec}}^{\mathrm{contact}}(V) = \Delta J_{\mathrm{extr,e}}^{\mathrm{anode}}(V) + \Delta J_{\mathrm{extr,h}}^{\mathrm{cathode}}(V), \quad (18)$$

while for $V > V_0$ it it is given by [see Fig. 1(b)]

$$\Delta J_{\mathrm{rec}}^{\mathrm{contact}}(V) = \left[\Delta J_{\mathrm{extr,h}}^{\mathrm{anode}}(V) - \Delta J_{\mathrm{inj,h}}^{\mathrm{anode}}(V)\right] + \left[\Delta J_{\mathrm{extr,e}}^{\mathrm{cathode}}(V) - \Delta J_{\mathrm{inj,e}}^{\mathrm{cathode}}(V)\right]. \quad (19)$$

Equation (19) shows that for $V > V_0$, the contact photorecombination is reduced by photoinduced injection current densities $\Delta J_{\mathrm{inj,h}}^{\mathrm{anode}}$ and $\Delta J_{\mathrm{inj,e}}^{\mathrm{cathode}}$. They denote the difference between the current densities injected from the contacts under illumination and in the dark,

$$\Delta J_{\mathrm{inj}}(V) = J_{\mathrm{inj,illum}}(V) - J_{\mathrm{inj,dark}}(V). \quad (20)$$

This difference originates from light induced variations of the charge-carrier distribution and the internal electric field. For $V < V_0$, i.e., in Eq. (18), the photoinduced injection current densities can be neglected because of the large energy barriers for electron injection at the anode and hole injection at the cathode [see Fig. 1(a)].

III. RESULTS AND DISCUSSION

For clarity and in order to be compatible with the line of argument presented in Ref. 9, only direct recombination [see Eq. (7)] was considered in Secs. III A and III B. Thus, notwithstanding Table I, the SRH lifetime τ_{SRH} in these sections was set to infinity. The influence of the trap assisted SRH recombination on the photocurrent density will be discussed in Sec. III D.

A. Influence of injection barriers

In a recent article it was found that, depending on the choice of cathode material and thus of the cathode injection barrier, the pseudosymmetric photocurrent-voltage characteristics $J_{\mathrm{ph}}(V)$ were shifted by an offset current density J_{POS}.[9] Increasing J_{POS} was presented as an option to increase the cell efficiency.[7–9] In this section, we investigate the influence of the contact injection barriers on $J_{\mathrm{ph}}(V)$ and compare the simulation results to experimental data from literature.

Figure 2 shows the simulated photocurrent-voltage characteristics $J_{\mathrm{ph}}(V)$ for different values of the injection barriers $\phi_{\mathrm{n,p}}$. The photocurrent density J_{ph} was split up into a minority $J_{\mathrm{ph,min}}$ and a majority $J_{\mathrm{ph,maj}}$ contribution. Figure 2(a) shows that large injection barriers of $\phi_{\mathrm{n,p}} = 0.4$ eV caused $J_{\mathrm{ph}}(V)$ to be nearly point symmetric with respect to $V_0 \approx 0.3$ V. For voltages $V < V_0$, J_{ph} was carried almost exclusively by majority charge carriers and saturated at the optically generated current density $|J_{\mathrm{ph,sat}}(V \ll V_0)| \approx J_{\mathrm{opt}}$. Approximately the same saturation value was observed for $V \gg V_0$, where minority charge carriers constituted the dominant contribution to J_{ph}. The large injection barriers $\phi_{\mathrm{n,p}} = 0.4$ eV resulted in high equilibrium concentrations n_0, p_0 and thus in low photorecombination rates for the minority charge carriers. As a result, the extraction of minority charge carriers was associated with recombination losses comparable to those which occurred during the extraction of majority charge carriers. Consequently, the photorecombination current density ΔJ_{rec} was found to be nearly symmetric with respect to the compensation voltage V_0. At $V = V_0$, all photogenerated charge carriers recombined and the photorecombination current density was equal to the optically generated current density $\Delta J_{\mathrm{rec}} = J_{\mathrm{opt}}$.

Figures 2(b) and 2(c) show $J_{\mathrm{ph}}(V)$ for lower values of the injection barriers $\phi_{\mathrm{n,p}}$. While the photocurrent density's saturation value at reverse bias $|J_{\mathrm{ph,sat}}(V \ll V_0)|$ was virtually not affected by the reduction of $\phi_{\mathrm{n,p}}$, the saturation current

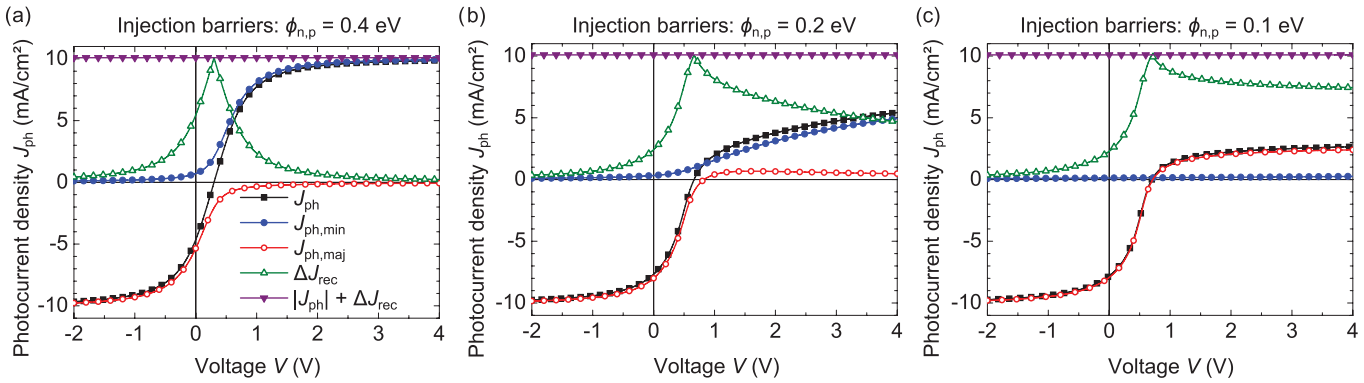

FIG. 2. (Color online) Simulated photocurrent-voltage characteristics $J_{\mathrm{ph}}(V)$ for different values of the injection barriers (a) $\phi_{\mathrm{n,p}} = 0.4$ eV, (b) $\phi_{\mathrm{n,p}} = 0.2$ eV, and (c) $\phi_{\mathrm{n,p}} = 0.1$ eV. The total photocurrent density J_{ph} is the sum of the minority $J_{\mathrm{ph,min}}$ and majority $J_{\mathrm{ph,maj}}$ charge-carrier contributions. The sum of $|J_{\mathrm{ph}}|$ and the photorecombination current density ΔJ_{rec} equals the optically generated current density J_{opt}. For the simulation, the SRH lifetime τ_{SRH} was set to infinity. Table I summarizes the remaining simulation parameters.

TABLE II. Parameters of the photocurrent-voltage characteristics $J_{ph}(V)$ shown in Fig. 2. The table lists the built-in voltage $qV_{bi} = E_g - \phi_n - \phi_p$, the compensation voltage V_0, the quasi-flat-band voltage V_{QFB} where the electric field in the center of the device vanishes, the voltage at the point of symmetry V_{POS}, and the current density $J_{POS} = J_{ph}(V_{POS})$.

	$\phi_{n,p} = 0.4$ eV	$\phi_{n,p} = 0.2$ eV	$\phi_{n,p} = 0.1$ eV
V_{bi}	0.30 V	0.70 V	0.90 V
V_0	0.30 V	0.66 V	0.70 V
V_{QFB}	0.30 V	0.64 V	0.66 V
V_{POS}	0.30 V	0.51 V	0.53 V
J_{POS}	0 mA cm^{-2}	−2.4 mA cm^{-2}	−2.6 mA cm^{-2}

density at forward bias $|J_{ph,sat}(V \gg V_0)|$ decreased by up to 75% at $\phi_{n,p} = 0.1$ eV. This result can be explained by an exponential decrease of the minority charge carriers' equilibrium concentrations n_0, p_0 and lifetimes τ_n, τ_p in the vicinity of the contacts, which is a direct consequence of the reduced injection barriers $\phi_{n,p}$ [see Eqs. (12) and (14)]. As a result, the photorecombination losses ΔJ_{rec} at $V > V_0$ significantly increased and exceeded those at $V < V_0$.

Another consequence of the reduced injection barriers was an increase of the majority charge-carrier photocurrent density $J_{ph,maj}$ at $V > V_0$. In the case of $\phi_{n,p} = 0.1$ eV, it was responsible for almost the total forward photocurrent density [see Fig. 2(c)]. At first glance, this observation seems to contradict the mechanism presented in Fig. 1(b), which states that for $V > V_0$, the photogenerated charge carriers are driven toward the contacts where they are minorities. The occurrence of this majority current density can be explained by the buildup of photogenerated minority charge carriers at the contacts. This charge accumulation altered the electric field and charge-carrier distribution and thus triggered the injection of additional majority charge carriers [see Eq. (20)]. The subsequent recombination of these additionally injected majorities and photogenerated minorities acts as a transformation of a minority photocurrent into a majority photocurrent. In order to corroborate this mechanism, the charge carriers' Coulomb interaction was deactivated by setting the dielectric constant to infinity $\epsilon_r = \infty$. To avoid side effects of ϵ_r on the direct recombination rate and thus on $J_{ph}(V)$, the value of k_{rec} was kept constant (see Table I) and not recalculated according to Eq. (8). Without Coulomb interaction no additional injection was observed. For $\phi_{n,p} = 0.1$ eV and $\epsilon_r = \infty$, the photocurrent density at $V > V_0$ was reduced to virtually zero while $J_{ph}(V < V_0)$, which consisted of minority charge carriers, was hardly affected (not shown).

Table II summarizes the influence of the injection barriers $\phi_{n,p}$ on the characteristic points of $J_{ph}(V)$. A decrease of the injection barriers $\phi_{n,p}$ increased the difference between the built-in voltage $qV_{bi} = E_g - \phi_n - \phi_p$ and V_0. This observation can be attributed to band bending at the contacts due to the low injection barriers.[9,37] At $V = V_0$, the photocurrent vanished because no effective driving force acted upon the photogenerated charge carriers. If contact band bending could be neglected and the charge-carrier generation was homogeneous, V_0 was equal to the quasi-flat-band voltage V_{QFB}. At V_{QFB} the electric field in the center of the device vanished and diffusion was the only driving force for the photogenerated charge carriers. A more detailed discussion on V_0 and V_{QFB} is presented in Sec. III C.

The point of symmetry (POS) was defined as the center point of inflection where the derivative dJ_{ph}/dV had an extremum.[8] In agreement with experimental results from Ref. 9, the model reproduced the shift of the POS by J_{POS} along the current density axis upon reduction of the injection barriers. In contrast to previous publications,[7,9] we propose that such a shift in J_{POS} is generally not beneficial for the device performance. Instead of an actual increase in the photocurrent density's saturation value $J_{ph,sat}$ under operation conditions, the simulation showed that the shift in J_{POS} was caused by increased photorecombination losses ΔJ_{rec} for voltages $V > V_0$. The obvious increase in device performance that occurred for decreased injection barriers (see Fig. 2) was due to the increased built-in voltage V_{bi}. It resulted in an enhanced open-circuit voltage V_{oc} and in more efficient charge extraction, i.e., in a higher short circuit current density J_{sc} and in this case also in a higher fill factor FF. An experimentally observed increase in $J_{ph,sat}$ upon the change of cathode material[9] does not contradict the presented modeling results because it is very likely not related to the change in work function. One explanation for the observed increase in $J_{ph,sat}$ (Ref. 9) is an unintentional annealing of the organic layer during thermal evaporation of the cathode. For the investigated donor/acceptor combination (P3HT:PCBM), it was shown that already a 4-min anneal at 75 °C can account for the observed increase in $J_{ph,sat}$.[38] Another possible explanation is damage to the active layer caused by the metal deposition.[39] The introduction of a thin Ca layer between active layer and the cathode[9] may have reduced the detrimental effects of the thermal metal evaporation and thus increased $J_{ph,sat}$. Note that the simulated photocurrent-voltage characteristics in this paper and the experimental data in Refs. 7–9 are mathematically not strictly symmetric, but exhibit an approximate point symmetry.

B. Influence of selective contacts

The increase of $J_{ph}(V > V_0)$ with increasing injection barriers, as shown in Fig. 2, was mainly due to an increased extraction of photogenerated minority charge carriers. Because in reality the surface recombination velocity S_{min} of minority charge carriers is finite,[40,41] or even assumed to be zero,[9] the extraction of minority charge carriers may be hampered or inhibited. In this section, we investigate the influence of self-selective contacts, i.e., $S_{min} = 0$, on $J_{ph}(V)$ for both small and large injection barriers. Although real contacts cannot be perfectly selective, we consider $S_{min} = 0$ as a limiting case and in order to be compatible with the simulations presented in Ref. 9.

1. *Large injection barriers*

Figure 3(a) shows $J_{ph}(V)$ for large injection barriers $\phi_{n,p} = 0.4$ eV and perfectly self-selective contacts, i.e., $S_{min} = 0$, which suppressed the minority charge-carrier currents at the contacts [see Eq. (10)]. For this reason, the total photocurrent density J_{ph} was equal to the majority current density $J_{ph,maj}$. The most prominent features were the three inflection points of $J_{ph}(V)$ as well as the broad and symmetric photorecombination peak at the compensation voltage $V_0 = 0.61$ V. Relative to

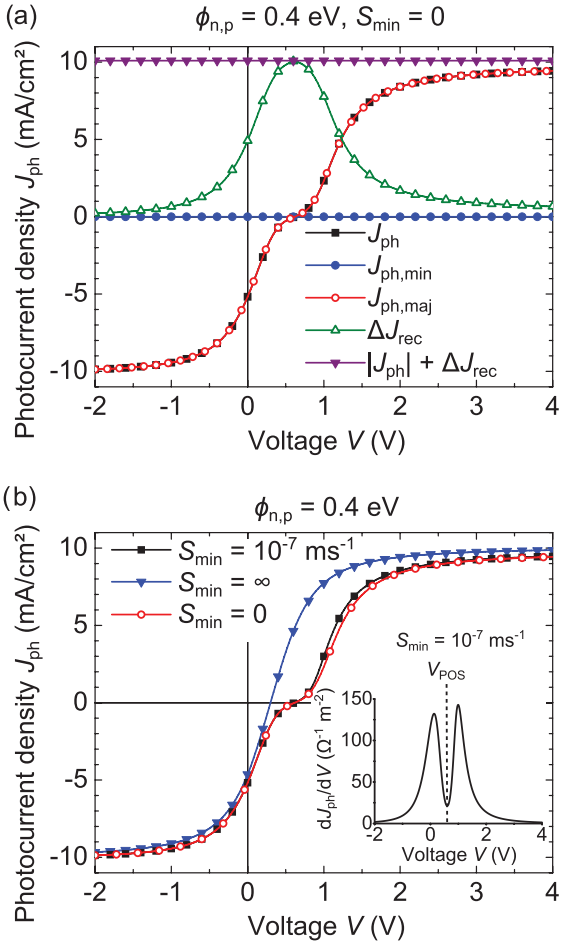

FIG. 3. (Color online) (a) Simulated photocurrent-voltage characteristics $J_{ph}(V)$ for injection barriers $\phi_{n,p} = 0.4$ eV and a minority charge-carrier surface recombination velocity $S_{min} = 0$. (b) Comparison of $J_{ph}(V)$ for $S_{min} = 0$, $S_{min} = 10^{-7}$ m s^{-1}, and $S_{min} = \infty$. The inset shows the derivative dJ_{ph}/dV for $S_{min} = 10^{-7}$ m s^{-1}.

the center point of inflection, which was located at $V_{POS} \approx V_0$, $J_{ph}(V)$ exhibited a pseudo point-symmetry with nearly equal absolute saturation values for forward and reverse bias.

Because the minority charge carriers could not pass the self-selective contacts, voltages above V_{bi} caused a buildup of minority charge carriers. Figure 3(b) shows that this charge buildup resulted in a diffusion potential, which acted against the applied voltage and raised the compensation voltage $V_0 = 0.61$ V by more than 100% compared to the case with nonselective contacts where $V_0 = V_{bi} = 0.3$ V (see Table II). Additionally, the charge buildup resulted in an increased photorecombination ΔJ_{rec} over a wide voltage range. At $V > V_0$ the band bending, caused by the buildup of photogenerated minority charge carriers, triggered the injection of additional majority charges at the contacts $\Delta J_{inj}(V)$. Similar to the discussion in Sec. III A, the subsequent recombination of photogenerated minority charges and injected majority charges was a nearly lossless transformation of the blocked minority photocurrent into a majority photocurrent.

The comparison to experimental data (Fig. 6 of Ref. 8) illustrates that the basic drift-diffusion model, which does not include any field dependent charge generation process, qualitatively reproduces $J_{ph}(V)$ and its derivative dJ_{ph}/dV. In contrast to Ref. 8, these results also indicate that the shape of dJ_{ph}/dV shown in the inset of Fig. 3(b) is not a clear indication for a field dependent exciton dissociation process in organic BHJ solar cells. We recently published a way to identify and quantitatively characterize a field dependent exciton dissociation process in merocyanine/C_{60} bilayer devices by varying the active layer thickness and the cell temperature.[15,16]

2. *Small injection barriers*

For small injection barriers $\phi_{n,p} = 0.1$ eV, selective contacts had nearly no effect on $J_{ph}(V)$ [compare Figs. 4(a) and 2(c)]. Figure 4(b) shows a direct comparison between the two photocurrent densities. It reveals that, except for minor deviations under reverse bias due to the reduced contact recombination for $S_{min} = 0$, the two curves overlap perfectly. In contrast to the case with large injection barriers $\phi_{n,p} = 0.4$ eV [see Fig. 3(b)], V_0 was unaffected by the change in S_{min}. This was due to the low lifetime of the minority charge

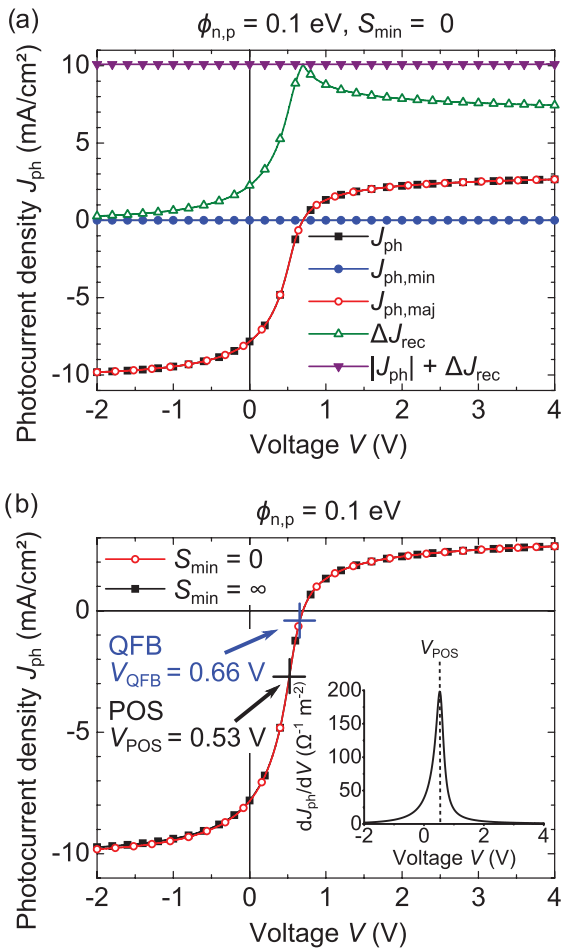

FIG. 4. (Color online) (a) Simulated photocurrent-voltage characteristics $J_{ph}(V)$ for injection barriers $\phi_{n,p} = 0.1$ eV and a minority charge-carrier surface recombination velocity $S_{min} = 0$. (b) Comparison of $J_{ph}(V)$ for $S_{min} = 0$ and $S_{min} = \infty$. In addition to the point of symmetry (POS) the quasi-flat band voltage V_{QFB} is marked. At this voltage the electric field in the center of the device vanishes (flat bands). The inset shows the derivative dJ_{ph}/dV.

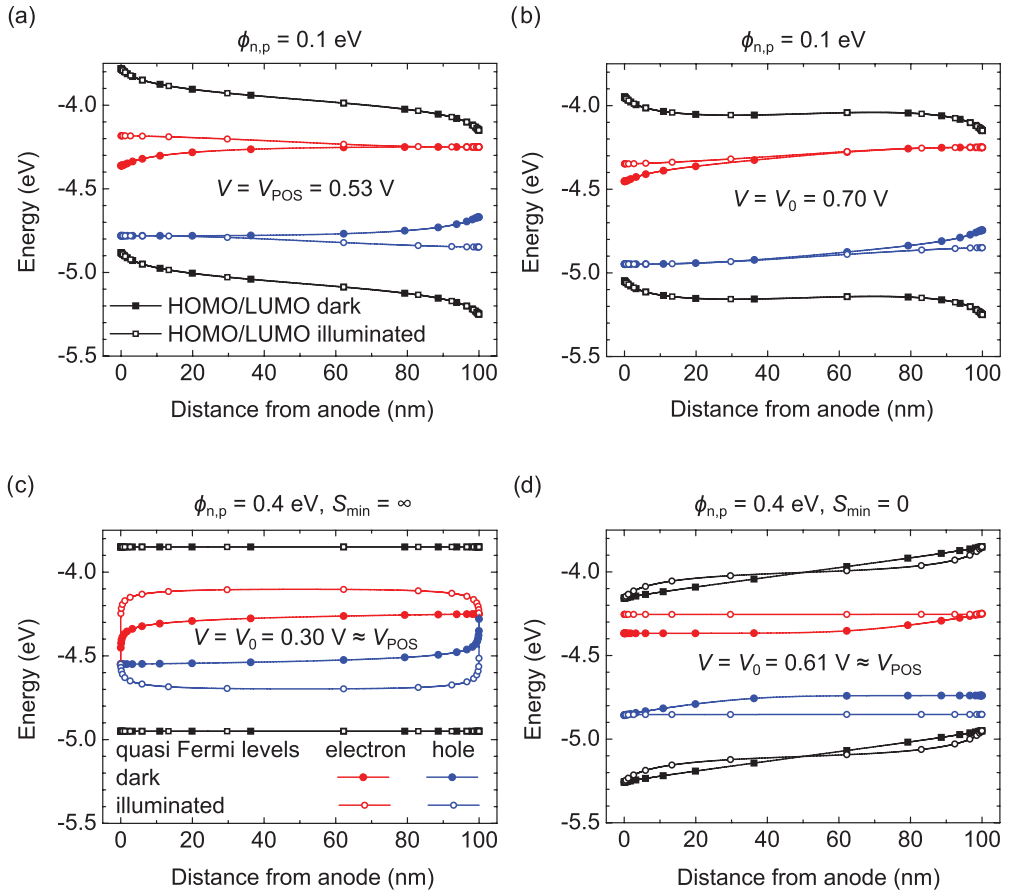

FIG. 5. (Color online) Simulated band diagrams and quasi-Fermi levels of dark and illuminated cells for (a), (b) $\phi_{n,p} = 0.1$ eV and (c), (d) $\phi_{n,p} = 0.4$ eV. For $\phi_{n,p} = 0.1$ eV, the results were found to be approximately independent of the minority charge-carrier surface recombination velocity S_{min}. The simulation parameters are summarized in Table I. For this simulation only direct recombination was considered, i.e., $\tau_{SRH} = \infty$.

carriers in the vicinity of the contacts, caused by the small injection barriers. It prevented an accumulation of minorities at the contacts and thus a significant diffusion potential.

In summary, if the lifetime of the minority charge carriers was sufficiently high to allow for a charge accumulation at the self-selective contacts, the resulting diffusion potential shifted the compensation voltage V_0 to values exceeding the built-in voltage V_{bi} [see Fig. 3(b)]. In contrast to the theory proposed in Ref. 7, the self-selective contacts did not influence the photocurrent density's offset J_{POS} at the point of symmetry (POS).

C. Point of symmetry and compensation voltage

The photocurrent-voltage curve $J_{ph}(V)$ has two characteristic points: the point of symmetry (POS), which is located at the center point of inflection of $J_{ph}(V)$, and the compensation voltage V_0, where the photocurrent density vanishes, i.e., $J_{ph}(V_0) = 0$. In order to get a deeper insight into the physical meaning of these characteristic points, we discuss simulated band diagrams for different sets of parameters.

Figures 5(a) and 5(b) show the energy levels calculated for small injection barriers $\phi_{n,p} = 0.1$ eV at $V_{POS} = 0.53$ V and $V_0 = 0.70$ V, respectively. The corresponding photocurrent-voltage characteristic $J_{ph}(V)$ and the set of model parameters are shown in Fig. 4 and in Table I, respectively. Due to the band bending caused by the low injection barriers,[37] both voltages were well below the built-in voltage $V_{bi} = 0.9$ V. At the compensation voltage $V_0 = 0.70$ V the photocurrent density vanished, i.e., $J_{ph}(V_0) = 0$. A small nonzero electric field in the device drove the charge carriers toward the contacts where they were minorities, i.e., electrons to the anode and holes to the cathode [see Fig. 5(b)]. The field compensated for a net extraction of majority charge carriers, which resulted in a negative photocurrent at quasi-flat band (QFB) conditions $V_{QFB} = 0.66$ V. This residual photocurrent at QFB conditions was caused by the contact band bending, which separated charges generated in the vicinity of the contacts. In this context, charge separation does not refer to the field assisted dissociation of charge-transfer states but to the separation of free charge carriers.

For P3HT:PCBM BHJ solar cells, Limpinsel *et al.*[9] investigated the relation between V_{POS} and V_{QFB}. They experimentally determined V_{POS} and V_{QFB} to be in the ranges 0.52–0.64 and 0.5–0.6 V, respectively. Due to the large slope of $J_{ph}(V)$ at voltages around V_{POS} [see the inset of Fig. 4(b)], the experimental uncertainty in the above-mentioned voltage ranges was too large to yield a clear relation between V_{POS} and V_{QFB}. For this reason, Limpinsel *et al.*[9] applied a drift-diffusion simulation using the parameters shown in Table I and found

that $V_{POS} = V_{QFB} = 0.66$ V. They explained this concurrence of the POS and QFB conditions by symmetric changes in driving force with applied bias at voltages around V_{QFB}.[9] Using their set of simulation parameters, we reproduced the QFB condition at 0.66 V but found $V_{POS} = 0.53$ V and thus 20% lower than V_{QFB} [see Fig. 4(b)]. This difference between V_{POS} and V_{QFB} can be explained by the different lifetimes of minority and majority charge carriers. By definition, at $V = V_{QFB}$ the electric field F inside the device is zero and $|F|$ changes nearly symmetrical with respect to small variations of the applied voltage V.[9] Despite this symmetry, $J_{ph}(V)$ does not generally exhibit a point-symmetric behavior around $V = V_{QFB}$ because the charge-carrier lifetimes $\tau_{n,p}$ and thus the photorecombination current density ΔJ_{rec} are not symmetric with respect to $V = V_{QFB}$ [see Fig. 4(a)]. Because the simulation model used in Ref. 9 is well documented and does most likely not contain any hidden parameters, the above-mentioned findings indicate that the simulation results in Ref. 9 as well as the corresponding discussion should be reexamined carefully.

Figure 5(c) shows a band diagram calculated at $V = V_0 = 0.3$ V for nonselective contacts ($S_{min} = \infty$) and large injection barriers ($\phi_{n,p} = 0.4$ eV). This highly symmetric device, i.e., the contacts were nonselective, the high injection barriers caused nearly no contact band bending, and the minority lifetime did not limit J_{ph} under forward bias conditions, resulted in a highly symmetric photocurrent-voltage characteristic [see Fig. 2(a)]. As a consequence, V_0, V_{POS}, and V_{QFB} all coincided with the built-in voltage $V_{bi} = 0.3$ V.

Figure 5(d) shows the band diagram for selective contacts ($S_{min} = 0$) and large injection barriers ($\phi_{n,p} = 0.4$ eV) calculated at $V = V_0 = 0.61$ V. The corresponding photocurrent-voltage characteristic $J_{ph}(V)$ is depicted in Fig. 3. Similar to the case in Fig. 5(c), the minority charge-carrier lifetimes $\tau_{n,p}$ did not limit $J_{ph}(V \gg V_0)$, and hence the POS and the compensation voltage V_0 coincided, i.e., $V_0 \approx V_{POS}$. However, V_0 exceeded the built-in voltage $V_{bi} = 0.3$ V by more than 100% due to the diffusion potential caused by the selective contacts. This diffusion potential manifested itself as a pronounced increase of the contact band bending upon illumination.

In summary, the photocurrent-voltage characteristics $J_{ph}(V)$ of bulk-heterojunction solar cells exhibit an approximate point symmetry with respect to a point of symmetry (POS), which was defined as the center point of inflection of $J_{ph}(V)$.[8] Our simulations showed that the voltage V_{POS} at which the POS occurs mainly depends on the recombination rate in the vicinity of the contacts and cannot be related to a specific value of the cell's internal electric field [compare Figs. 5(a), 5(c), and 5(d)]. Thus, aside from the above-mentioned definition, we propose that the POS has no further physical meaning. If the compensation voltage V_0 is applied to the cell, no effective driving force acts upon the photogenerated charge carriers, resulting in $J_{ph}(V_0) = 0$. For a symmetric device with large injection barriers and negligible contact band bending, a vanishing driving force is equivalent to flat bands in the bulk of the device [see Fig. 5(c)]. If asymmetries other than a built-in field are present, e.g., selective contacts or contact band bending, the electric field in the center of the device has a nonzero value at $V = V_0$ [see Fig. 5(d)].

D. Recombination via trap states

The preceding sections discussed the photocurrent in the context of direct recombination [see Eq. (7)]. However, recent publications demonstrated that a direct recombination mechanism alone was not sufficient to reproduce experimental data of organic HJ solar cells.[27,36] Instead, the experimental results were found to be compatible with a recombination mechanism via trap states located within the energy-band gap.[27,36,42–44] Numerical and analytical models employing a trap recombination mechanism reproduced experimental current-voltage characteristics including the ideality factor[25,27,45] as well as charge extraction experiments.[27] This section discusses the effect of recombination via trap states on $J_{ph}(V)$ using the Shockley-Read-Hall (SRH) recombination mechanism calculated for a single deep defect.[28,29]

In contrast to the direct recombination mechanism, the SRH lifetime τ_{SRH} of minority charge carriers is constant, independent of the charge carriers' equilibrium concentrations, and thus independent of their position inside the device. Figure 6 shows that, for large injection barriers of $\phi_{n,p} = 0.4$ eV, the SRH recombination caused a symmetric reduction of $|J_{ph}|$ around the compensation voltage V_0. Small injection barriers $\phi_{n,p} = 0.1$ eV resulted in a similar reduction of $|J_{ph}|$ for voltages $V < V_0$, while nearly no effect occurred for $V > V_0$ (see Fig. 6). Here, the SRH recombination had very little influence because at $V > V_0$ the direct recombination mechanism dominated the photorecombination ΔJ_{rec} due to the low minority charge-carrier lifetime τ_{min} at the contacts.

For shallow trap states, e.g., band tails, which are located less than $3k_BT$ from the band edge, the re-emission of trapped charge carriers into the bands reduces the SRH recombination rate compared to Eq. (9). However, the trends shown in Fig. 6 remain valid because the re-emission coefficients do not depend on the concentrations of free charge carriers n, p.[27,46] In organic semiconductors, the band-tail states do not only promote recombination but also accommodate a

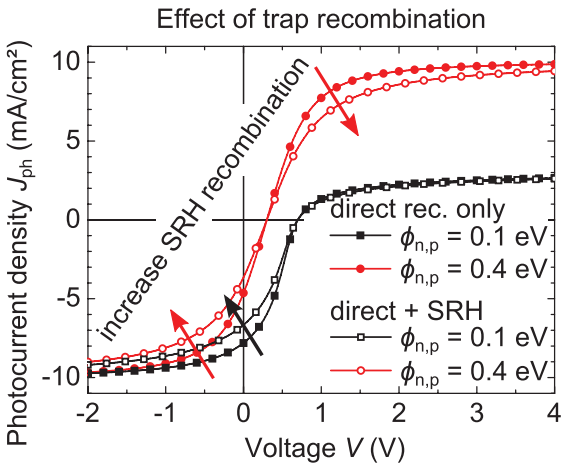

FIG. 6. (Color online) Simulated photocurrent-voltage characteristics $J_{ph}(V)$ with (open symbols) and without $\tau_{SRH} = \infty$ (solid symbols) SRH recombination. The effect of the SRH recombination depends on the value of the injection barriers $\phi_{n,p}$. Table I summarizes the simulation parameters.

significant amount of space charge. Similar to the equilibrium concentrations of the free charge carriers, the amount and sign of the tails states' space charge depends on the position inside the device. Close to the cathode, mainly trapped electrons occupy the tail states while trapped holes dominate in the vicinity of the anode. This additional space charge increases the contact band bending, which reduces the value of the electric field in the center of the cell and shifts V_0 toward lower voltages. Because trapped charge carriers are no longer subject to direct recombination according to Eq. (7), the introduction of tail states can also affect the direct recombination rate. Simulation results for exponential band tails including spatial concentration profiles for free and trapped charge carriers can be found in the Supplemental Material.[47]

These findings indicate that, even if recombination via trap states is the major loss factor under normal operating conditions, optimized (small) injection barriers can cause the direct recombination to significantly influence the photocurrent losses at voltages above the compensation voltage V_0. Because the trap recombination did not introduce fundamental symmetry changes of $J_{ph}(V)$, the aspects discussed in the previous sections, especially the position dependent charge-carrier lifetimes, remain valid.

E. Effect of the series resistance

Another important parameter influencing the photocurrent-voltage characteristic $J_{ph}(V)$ is the series resistance R_s. The influence of R_s on $J_{ph}(V)$ is well known since the 1960s.[48,49] In the field of crystalline silicon solar cells, the comparison of dark and light current-voltage characteristics constitutes an accurate method to determine the value of R_s.[50] Recently, Street *et al.*[51] revisited the topic in the context of organic solar cells and applied an external series resistance $R_{s,ext}$ to a PCTBT/PC$_{70}$BM solar cell. In agreement with calculations based on an equivalent circuit model, they found $R_{s,ext} \geqslant 5\ \Omega\,\mathrm{cm}^2$ to cause a significant reduction of $|J_{ph}|$. The reduction was found to be most pronounced for voltages exceeding the compensation voltage V_0 because the high current densities in this voltage range resulted in high resistive losses ΔV_{loss} at the series resistance. Because ΔV_{loss} occurred outside the active layer, the voltage drop at the internal diode was reduced and less driving force for the photogenerated charge carriers was available.[51] The authors concluded that such series resistance effects were an alternative and likely explanation for the experimentally observed[7–9] shift of $J_{ph}(V)$ along the current density axis.[51] In this section, we apply the drift-diffusion model to study the effect of R_s on $J_{ph}(V)$.

Figure 7(a) shows the current-voltage characteristics $J_{dark}(V)$ of nonilluminated cells. Increasing the injection barriers $\phi_{n,p}$ from 0.1 to 0.2 eV reduced the concentrations n, p of mobile charge carriers in the device [see Eqs. (11) and (12)]. As a result, the conductivity $\rho = q(n\mu_n + p\mu_p)$ decreased and the intrinsic series resistance $R_{s,int}$ increased. The same resistive effect on J_{dark} was observed for a cell with $\phi_{n,p} = 0.1$ eV and an additional external series resistance $R_{s,ext} = 6\ \Omega\,\mathrm{cm}^2$ [see Fig. 7(a)]. Figure 7(b) shows the three corresponding photocurrent-voltage characteristics $J_{ph}(V)$. In agreement with the predictions by Street *et al.*,[51] the external series resistance $R_{s,ext}$ reduced $J_{ph}(V)$ for $V > V_0$.

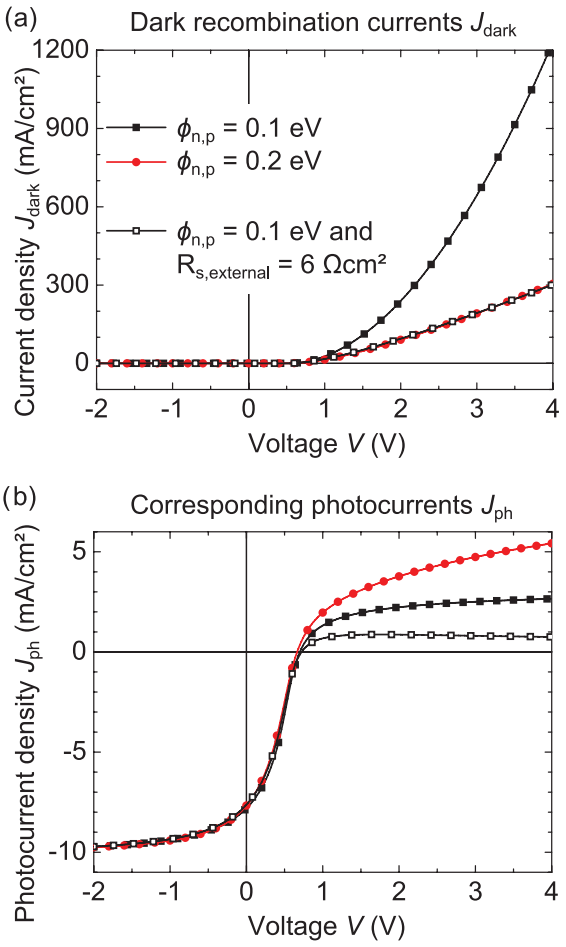

FIG. 7. (Color online) (a) Simulated current-voltage characteristics $J_{dark}(V)$ of nonilluminated cells. (b) Corresponding photocurrent-voltage characteristics $J_{ph}(V)$. The comparison shows that the series resistance $R_s = 1/[dJ_{dark}(V)/dV]$ did not correlate with the shape of $J_{ph}(V)$.

However, no clear correlation existed between the total series resistance determined from the dark J-V characteristics $R_s = 1/(dJ_{dark}(V)/dV)$ and the shape of $J_{ph}(V)$.

This discrepancy can be explained by the difference between external and intrinsic series resistances. An external series resistance $R_{s,ext}$, which was also assumed by Street *et al.*,[51] causes a voltage drop outside the active layer. This lowers the potential difference inside the active layer and thus reduces the driving force for the collection of photogenerated charge carriers. As a result, $R_{s,ext}$ reduces the absolute value of the photocurrent density $|J_{ph}|$. An intrinsic series resistance $R_{s,int}$ is the result of the active material's finite conductivity ρ and causes a voltage drop inside the active layer. Consequently, $R_{s,int}$ has no detrimental effect on the field driven charge-carrier collection, which takes place in the intrinsic absorber layer of organic HJ solar cells and other pin-type devices. One way to alter the materials conductivity $\rho = q(n\mu_n + p\mu_p)$ and thus $R_{s,int}$ is a change of the charge-carrier concentrations n, p, e.g., via the injection barriers $\phi_{n,p}$. Figure 7 shows that an increase of $\phi_{n,p}$ simultaneously increased $R_s = 1/[dJ_{dark}(V)/dV]$ and, as described in Sec. III A, $J_{ph}(V > V_0)$. The intrinsic series resistance $R_{s,int}$ was also affected by changes of the mobilities

μ_n and μ_p while $J_{ph}(V)$ remained unaffected as long as the mobility-lifetime product $\mu\tau$ and thus the charge extraction efficiency was not changed (not shown).

In summary, external series resistances $R_{s,ext}$ reduce the voltage drop over the solar cell's active layer and thus lower the photocurrent density's saturation value $J_{ph,sat}$ for $V > V_0$. Although $R_{s,ext}$ can result in an apparent shift of $J_{ph}(V)$, it cannot explain the experimentally observed cathode dependence of $J_{ph}(V)$,[9] and does not contradict the line of argument presented in Sec. III A. A significant external series resistance, which dominates the total series resistance, can, in principle, be avoided by proper contacting. Intrinsic series resistances $R_{s,int}$ do not reduce the voltage drop over the active layer and do not affect $J_{ph}(V)$ as long as the mobility-lifetime product $\mu\tau$ is sufficiently high.

IV. CONCLUSION

We have studied the approximately point-symmetric photocurrent-voltage characteristics $J_{ph}(V)$ of bulk-heterojunction (BHJ) solar cells by means of a drift-diffusion based device simulation model. Our results indicate that position dependent charge-carrier lifetimes $\tau_{n,p}$, caused by a direct recombination mechanism, result in different extraction efficiencies for minority and majority charge carriers. Based on this fundamental principle for solar cells with intrinsic absorber layers, our model reproduced recently published experimental data without the need of a field dependent exciton dissociation mechanism or other additional parameters. We discussed the characteristic points of $J_{ph}(V)$: the compensation voltage V_0 where the photocurrent density vanishes, i.e., $J_{ph}(V_0) = 0$, the quasi-flat band (QFB) voltage V_{QFB}, and the point of symmetry (POS).

Although, the electric field in the center of the cell vanishes at $V = V_{QFB}$, other driving forces like diffusion due to selective contacts or an electric field in the band bending regions close to the contacts can still result in $|J_{ph}| > 0$. Thus the QFB condition occurs at a voltage close to, but generally not equal to, V_0. In contrast to previous publications, we found that the POS is not a meaningful physical quantity and can generally not be related to the QFB condition. Because the current density J_{POS} at the POS does not have to be related to actual changes in the photocurrent density's saturation value $J_{ph,sat}$, increasing J_{POS} constitutes no option for device optimization.

ACKNOWLEDGMENTS

We would like to thank Stefan Schäfer for carefully reading the manuscript and the BMBF for the financial support in the framework of the OPEG project (13N9715). T.K. acknowledges support by an Imperial College Junior Research Fellowship.

*andreas.petersen@de.bosch.com

[1] M. A. Green, K. Emery, Y. Hishikawa, and W. Warta, Prog. Photovolt.: Res. Appl. **19**, 84 (2011).
[2] C. Deibel and V. Dyakonov, Rep. Prog. Phys. **73**, 096401 (2010).
[3] P. Würfel, *Physics of Solar Cells* (Wiley-VCH, Weinheim, 2005).
[4] T. Kirchartz, K. Ding, and U. Rau, in *Advanced Characterization Techniques for Thin Film Solar Cells* (Wiley-VCH, Weinheim, 2011), pp. 33–60, [http://dx.doi.org/10.1002/9783527636280.ch2].
[5] T. Kirchartz, J. Mattheis, and U. Rau, Phys. Rev. B **78**, 235320 (2008).
[6] V. D. Mihailetchi, L. J. A. Koster, J. C. Hummelen, and P. W. M. Blom, Phys. Rev. Lett. **93**, 216601 (2004).
[7] Z. E. Ooi, R. Jin, J. Huang, Y. F. Loo, A. Sellinger, and J. C. deMello, J. Mater. Chem. **18**, 1644 (2008).
[8] Z. E. Ooi, T. L. Tam, A. Sellinger, and J. C. de Mello, Energy Environ. Sci. **1**, 300 (2008).
[9] M. Limpinsel, A. Wagenpfahl, M. Mingebach, C. Deibel, and V. Dyakonov, Phys. Rev. B **81**, 085203 (2010).
[10] S. R. Cowan, A. Roy, and A. J. Heeger, Phys. Rev. B **82**, 245207 (2010).
[11] G. F. A. Dibb, T. Kirchartz, D. Credgington, J. R. Durrant, and J. Nelson, J. Phys. Chem. Lett. **2**, 2407 (2011).
[12] X. Wei, M. Raikh, Z. V. Vardeny, Y. Yang, and D. Moses, Phys. Rev. B **49**, 17480 (1994).
[13] G. G. Malliaras, J. R. Salem, P. J. Brock, and J. C. Scott, J. Appl. Phys. **84**, 1583 (1998).
[14] H. Frohne, S. E. Shaheen, C. J. Brabec, D. C. Müller, N. S. Sariciftci, and K. Meerholz, Chem. Phys. Chem. **3**, 795 (2002).
[15] A. Ojala, A. Petersen, A. Fuchs, R. Lovrincic, C. Pölking, J. Trollmann, J. Hwang, C. Lennartz, H. Reichelt, H. W. Höffken, A. Pucci, P. Erk, T. Kirchartz, and F. Würthner, Adv. Funct. Mater. **22**, 86 (2012).
[16] A. Petersen, A. Ojala, T. Kirchartz, T. A. Wagner, F. Würthner, and U. Rau(unpublished).
[17] J. A. Barker, C. M. Ramsdale, and N. C. Greenham, Phys. Rev. B **67**, 075205 (2003).
[18] L. J. A. Koster, E. C. P. Smits, V. D. Mihailetchi, and P. W. M. Blom, Phys. Rev. B **72**, 085205 (2005).
[19] G. A. Buxton and C. N., Modell. Simul. Mater. Sci. Eng. **15**, 13 (2007).
[20] T. Kirchartz, B. E. Pieters, K. Taretto, and U. Rau, J. Appl. Phys. **104**, 094513 (2008).
[21] J. Williams and A. B. Walker, Nanotech. **19**, 424011 (2008).
[22] I. Hwang, C. R. McNeill, and N. C. Greenham, J. Appl. Phys. **106**, 094506 (2009).
[23] R. Häusermann, E. Knapp, M. Moos, N. A. Reinke, T. Flatz, and B. Ruhstaller, J. Appl. Phys. **106**, 104507 (2009).
[24] A. Wagenpfahl, D. Rauh, M. Binder, C. Deibel, and V. Dyakonov, Phys. Rev. B **82**, 115306 (2010).
[25] S. Schäfer *et al.*, Phys. Rev. B **83**, 165311 (2011).
[26] P. Langevin, Ann. Chim. Phys. **28**, 433 (1903).
[27] T. Kirchartz, B. E. Pieters, J. Kirkpatrick, U. Rau, and J. Nelson, Phys. Rev. B **83**, 115209 (2011).
[28] R. N. Hall, Phys. Rev. **87**, 387 (1952).
[29] W. Shockley and W. T. Read Jr., Phys. Rev. **87**, 835 (1952).
[30] C. L. Braun, J. Chem. Phys. **80**, 4157 (1984).

[31]C. G. Shuttle, R. Hamilton, B. C. ORegan, J. Nelson, and J. R. Durrant, Proc. Natl. Acad. Sci. USA **107**, 16448 (2010).
[32]R. A. Street, S. Cowan, and A. J. Heeger, Phys. Rev. B **82**, 121301 (2010).
[33]R. Mauer, I. A. Howard, and F. Laquai, J. Phys. Chem. Lett. **1**, 3500 (2010).
[34]R. C. I. MacKenzie, T. Kirchartz, G. F. A. Dibb, and J. Nelson, J. Phys. Chem. C **115**, 9806 (2011).
[35]M. Zeman, J. van den Heuvel, B. E. Pieters, M. Kroon, and J. Willemen, *Advanced Semiconductor Analysis* (TU Delft, Delft 2003).
[36]R. A. Street, M. Schoendorf, A. Roy, and J. H. Lee, Phys. Rev. B **81**, 205307 (2010).
[37]M. Kemerink, J. M. Kramer, H. H. P. Gommans, and R. A. J. Janssen, Appl. Phys. Lett. **88**, 192108 (2006).
[38]F. Padinger, R. S. Rittberger, and N. S. Sariciftci, Adv. Funct. Mater. **13**, 85 (2003).
[39]P. Peumans, A. Yakimov, and S. R. Forrest, J. Appl. Phys. **93**, 3693 (2003).
[40]J. C. Scott and G. G. Malliaras, Chem. Phys. Lett. **299**, 115 (1999).
[41]A. Wagenpfahl, C. Deibel, and V. Dyakonov, J. Sel. Top. Quantum Electron. **16**, 1759 (2010).
[42]R. A. Street, Phys. Rev. B **84**, 075208 (2011).
[43]G. Garcia-Belmonte, P. P. Boix, J. Bisquert, M. Lenes, H. J. Bolink, A. La Rosa, S. Filippone, and N. Martín, J. Phys. Chem. Lett. **1**, 2566 (2010).
[44]G. Garcia-Belmonte, P. P. Boix, J. Bisquert, M. Sessolo, and H. J. Bolink, Sol. Energy Mater. Sol. Cells **94**, 366 (2010).
[45]N. C. Giebink, G. P. Wiederrecht, M. R. Wasielewski, and S. R. Forrest, Phys. Rev. B **82**, 155305 (2010).
[46]B. E. Pieters, K. Decock, M. Burgelman, R. Stangl, and T. Kirchartz, in *Advanced Characterization Techniques for Thin Film Solar Cells* (Ref. 4), pp. 501–527, [http://dx.doi.org/10.1002/9783527636280.ch19].
[47]See Supplemental Material at http://link.aps.org/supplemental/10.1103/PhysRevB.85.045208 for simulation results on tail state recombination.
[48]M. Wolf and H. Rauschenbach, Adv. Energy Conv. **3**, 455 (1963).
[49]R. J. Handy, Solid-State Electron. **10**, 765 (1967).
[50]A. G. Aberle, S. R. Wenham, and M. A. Green, in *Photovoltaic Specialists Conference, 1993, Conference Record of the Twenty Third IEEE* (IEEE, Louisville, KY , USA, 1993), pp. 133–139.
[51]R. A. Street, K. W. Song, and S. Cowan, Organic Electron. **12**, 244 (2011).